Advances in Applied Mathematics and Mechanics
Adv. Appl. Math. Mech., Vol. **15**, No. 5, pp. 1315-1334

DOI: 10.4208/aamm.OA-2021-0316
October 2023

Impacts of Down-Up Hill Segment on the Threshold of Shock Formation of Ring Road Vehicular Flow

Zejing Hu[1,3], M. N. Smirnova[2,*], N. N. Smirnov[2], Yongliang Zhang[1] and Zuojin Zhu[1,2,*]

[1] *Faculty of Engineering Science, University of Science and Technology of China, Hefei, Anhui 230026, China*
[2] *Faculty of Mechanics and Mathematics, Lomonosov Moscow State University, Moscow, 119992, Russia*
[3] *Anhui Xiang Shui Jian Pumped Storage Co., LTD, Wuhu, Anhui 241083, China*

Received 10 October 2021; Accepted (in revised version) 28 March 2022

Abstract. The study of impacts of down-up hill road segment on the density threshold of traffic shock formation in ring road vehicular flow is helpful to the deep understanding of sags' bottleneck effect. Sags are freeway segments along which the gradient increases gradually in the traffic direction. The main aim of this paper is to seek the density threshold of shock formation of vehicular flow in ring road with down-up hill segment, because down-up hill roadway segment is a source to cause capacity reduction that is an attractive topic in vehicular traffic science. To seek the density threshold numerically, a viscoelastic continuum model [1] is extended and used. To solve the model equations, a fifth-order weighted essentially non-oscillatory scheme for spatial discretization, and a 3rd order Runge-Kutta scheme for time partial derivative term are used. Validation by existing observation data and the Navier-Stokes like model [2] extended as EZM is done before conducting extensive numerical simulations. For ring road vehicular flow with three separated down-up hill segments, it is found that the density threshold of shock formation decreases monotonically with the relative difference of free flow speed, this variation can be simply fitted by a third order polynomial.

AMS subject classifications: 35Q80, 76A02

Key words: Down-up hill road segment, viscoelastic continuum model, sags' bottleneck effect, density threshold, WENO5 scheme.

1 Introduction

To investigate the effects of road infrastructure condition on traffic flow dynamics, a research background has been given in [1], from which the existing results of several stud-

*Corresponding author.
Emails: wonrims@inbox.ru (M. Smirnova), zuojin@ustc.edu.cn (Z. Zhu)

ies reported in [3–8] can be sought.

However, less work has been done for the down-up hill segment effects on the density threshold of traffic shock formation in ring road vehicular flow from macroscopic points of view. Therefore, by assuming that traffic sound speed of traffic flow at a state over second critical point is just equal to the second critical sound speed, this paper extends the macroscopic viscoelastic continuum model (VEM) reported in [1] and uses the extended model to predict the density threshold of traffic shock formation and travel time numerically. The ring road is composed of three separated down-up hill segments and horizontal road segment, as shown in Fig. 1. As the down segment is linked immediately by a length-identical uphill, thus we call the composed as the down-up hill segment or the sag. Indeed, due to the role of gravitational acceleration, there is a shorter braking distance for vehicles on uphill segment, but a longer braking distance for vehicles on downhill segment, with the vehicles on horizontal segment having a braking distance between the two. Generally, braking distance is a function of free flow speed [9]. Consequently, there should have three relevant free flow speeds on the three road segments. Therefore, for the ring road with down-up hill segment, the traffic fundamental diagram is section dependent, as shown in Fig. 2.

To validate the VEM, the existing observation data are used for comparison of traffic flow states, and the Navier-Stokes like model of Zhang [2] extended as EZM [10] is adopted to provide the counterpart results for validation. It is assumed that the total length of the ring road is 120km, and the single downhill or uphill length is 1km.

The main aim of this paper is to seek the density threshold of shock formation of vehicular flow in ring road with down-up hill segment. Hence, on the basis of the VEM, a fifth-order weighted essentially non-oscillatory scheme (WENO5) [11,12] and a third-order Runge-Kutta scheme (RK3) [13,14] are used to build a simulation platform. Model validation is done before conducting extensive numerical simulations of ring road vehicular flow to explore the density threshold and its variation trend. We will introduce the VEM and numerical method just before method of travel time prediction, then discuss the results, and finally give the conclusions.

2 Viscoelastic traffic flow model

The viscoelastic traffic flow model (VEM) [1] uses traffic pressure derived by assuming the explicit algebraic form of traffic sound speed and the definition of the sound speed in classical mechanics, rather than governed by a partial differential equation in the gas-kinetic-based model [15,16]. Assuming traffic density ρ is normalized by traffic jam density ρ_m, when velocity scale is v_0, the traffic flow rate q has a unit of $\rho_m v_0$. For length scale l_0, time scale is $t_0 = l_0/v_0$. Taking normalized traffic density ρ and normalized traffic flow rate q as mandatory variables, neglecting ramp effects, and defining traffic elasticity by

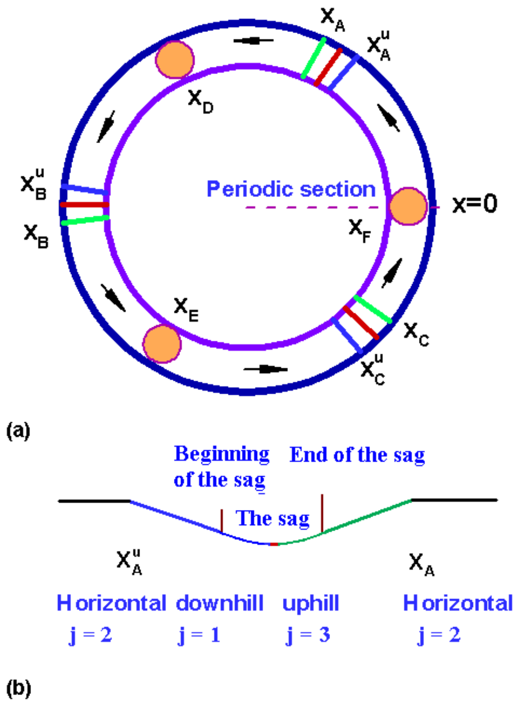

Figure 1: (a) Schematic diagram of ring traffic flow with three initial jams located at $x_J = 40,80,120$km for $J = \mathrm{D,E,F}$; (b) Road segments labeled by $j = 1,2,3$. Note that the downhill segment initiates at X_I^{u} and terminates by the subsequent uphill segment ending at X_I, thus the length of the downhill or uphill segment can be calculated by $L_{\mathrm{h}} = (X_I - X_I^{\mathrm{u}})/2$, for $I = \mathrm{A,B,C}$.

$\gamma = 0.68\nu\tau$, the non-dimensional form of VEM equations are

$$\begin{cases} \rho_t + q_x = 0, \\ \rho(u_t + uu_x) = R, \end{cases} \tag{2.1}$$

where R satisfies the expression (Zhu and Yang [21]; Ma et al. [22])

$$R + [\rho\gamma(R/\rho)_x]_x = (q_e - q)/\tau - p_x + [\rho(\nu+\nu_1)u_x]_x, \tag{2.2}$$

where the traffic elasticity is denoted by γ, $\rho\nu_1 = 3\rho\gamma u_x$, $p_x (= c^2\rho_x)$ is the gradient of traffic pressure, c is traffic sound speed, q_e is equilibrium traffic flow rate obtained by fundamental diagram as shown in Fig. 2, R/ρ is traffic flow acceleration, ν is the kinematic viscosity of traffic flows, with τ denoting the relaxation time of traffic flow. When the road is empty, the viscosity ν is zero. The term $[\rho(\nu+\nu_1)u_x]_x$ in the right hand side of Eq. (2.2) reflects some properties of traffic self-organization. In reality, ahead of a vehicle a speed increase tends to produce a positive value of u_{xx}, and thus provides drivers' motivation for acceleration, as the density reduction ahead of the vehicle can be foreseen in congested traffic flows.

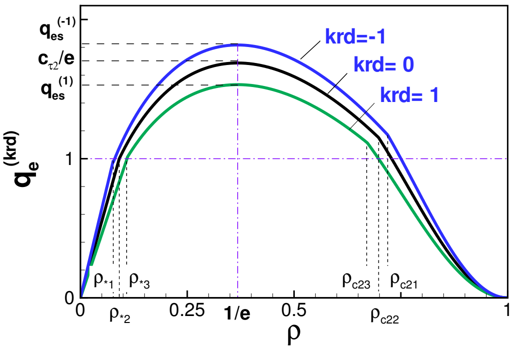

Figure 2: Fundamental diagram for traffic flows on a ring road with downhill (krd$=-1$), horizontal (krd$=0$), and uphill (krd$=1$) segments. Note that ρ is measured by jam density ρ_m, the flow rate $q_e^{(\mathrm{krd})}$ is measured by $\rho_{*2}v_{f2}$, and $q_{es}^{(\mathrm{krd})}=c_{\tau_j}/e\cdot[\rho_{*j}v_{fj}/\rho_{*2}v_{f2}]$, $\mathrm{krd}=j-2=-1,0,1$ for $j=1,2,3$ respectively.

The equilibrium traffic flow rate q_e on road segment j is denoted by $q_e^{(\mathrm{krd})}$, $\mathrm{krd}=j-2$, as shown in Fig. 2. Using traffic jam density ρ_m, the equilibrium flow rate in the VEM is expressed by

$$q_e^{(\mathrm{krd})}=\begin{cases}\rho v_{fj} & \text{for } \rho\in[0,\rho_{*j}],\\ -c_{\tau j}\rho\ln(\rho/\rho_m) & \text{for } \rho\in(\rho_{*j},\rho_{c2j}],\\ B_j\rho\{1-\mathrm{sech}[\Lambda_j\ln(\rho/\rho_m)]\} & \text{for } \rho\in(\rho_{c2j},\rho_m],\end{cases}\tag{2.3}$$

where ρ_{*j} is the first critical density, i.e., the corresponding maximum permissible density, over which the traffic flow becomes unstable. ρ_{c2j} is the second critical density, over which the traffic flow becomes stable again. At the second critical density ρ_{c2j}, traffic flow has an equilibrium speed u_{c2}. When the speed is used to define a ratio $\Lambda_j=c_{\tau j}/u_{c2}$, the parameter B_j can be written as

$$B_j=u_{c2j}/\{1-\mathrm{sech}[\Lambda_j\ln(\rho_{c2j}/\rho_m)]\}.\tag{2.4}$$

For the braking distance X_{brj}, the corresponding maximum permissible density ρ_{*j} at free flow speed v_{fj} is given by

$$\rho_{*j}=\rho_m\exp(-v_{fj}/c_{\tau j}).\tag{2.5}$$

As safe traffic density (ρ_{*j}) itself implies that the distance between vehicles are not shorter than the braking distance X_{brj}, denoting average vehicle length by l, then ρ_{*j} is defined by

$$\rho_{*j}=\rho_m[1+X_{\mathrm{brj}}/l]^{-1}.\tag{2.6}$$

Combining Eq. (2.5) and Eq. (2.6), we have

$$c_{\tau j}=v_{fj}/\ln[1+X_{\mathrm{brj}}/l].\tag{2.7}$$

Table 1: Parameters of traffic flow on ring road.

v_{f1}(km/h)	130	Λ_1	2.9187	l_0(m)	100
v_{f2}(km/h)	120	Λ_2	2.7802	$X_{\mathrm{A}}^{\mathrm{u}}$(km)	19
v_{f3}(km/h)	110	Λ_3	2.6398	$X_{\mathrm{B}}^{\mathrm{u}}$(km)	59
X_{br1}(m)	87	ρ_{*1}	0.08421	$X_{\mathrm{C}}^{\mathrm{u}}$(km)	99
X_{br2}(m)	80	ρ_{*2}	0.09090	L(km)	120
X_{br3}(m)	73	ρ_{*3}	0.09877	L_{h}(km)	1
τ_{01}(s)	6.6403	ρ_{c21}	0.70991	ρ_m(veh/km)	124
τ_{02}(s)	7.1937	ρ_{c22}	0.69790	l(m)	8.0
τ_{03}(s)	7.8477	$\rho_{c23}{}^{\dagger}$	0.68466	u_{c2}(km/h)	18
$c_{\tau 1}$	4.8159	X_{A}(km)	21	$v_0(=\rho_{*2}v_{f2})$(m/s)	3.03
$c_{\tau 2}$	4.5874	X_{B}(km)	61	$t_0(=l_0/v_0)$(s)	33
$c_{\tau 3}{}^{*}$	4.3556	X_{C}(km)	101		

$*$ $c_{\tau 1}$, $c_{\tau 2}$, and $c_{\tau 3}$ are in the unit of v_0.

† ρ_{*1}, ρ_{*2}, ρ_{*3}, ρ_{c21}, ρ_{c22}, and ρ_{c23} are in the unit of ρ_m.

It is noted that for the relaxation time of traffic flow τ, its definition is the same as that given by Zhang et al. [10]. As shown in Fig. 2, the fundamental diagrams labeled by segment index $krd=-1$, 0, 1 are obtained using the free flow speeds v_{fj} and the braking distances $X_{\mathrm{br}j}$, for $j=1$, 2, 3, their values can be seen in Table 1. The subscript 'j' is used to label some variables on downhill segment (j=1), horizontal segment (j=2), and uphill segment ($j=3$) respectively (see Fig. 1). The equilibrium flow-density relation relevant to the three situations described by Eq. (2.3) is assumed with respect to the existence of second critical phenomenon observed in traffic reality. On the ring road with three down-up hill segments, the uphill length is identical to the downhill length, given by $L_{\mathrm{h}}=(X_I-X_I^{\mathrm{u}})/2$, ($I$=A, B, C). Considering the gravitational effect of vehicles, naturally the free flow speed on downhill segment is larger but free speed on uphill segment is smaller, with free flow speed on the horizontal segment between the two, as shown in Table 1.

Similar to that reported previously [10], by assuming that on empty road traffic sound speed is exactly equal to the free flow speed, using pressure model parameter obtained by postulating that the sound speed at the second critical point is exactly equal to the speed $c_{\tau j}$, and defining

$$\left.\begin{aligned}
&K_j=\{c_{\tau j}[1-\alpha\rho_{c2j}/\rho_m]\}^2,\\
&c_{*j}^2=K_j/(1-\alpha\rho_{*j}/\rho_m)^2,\\
&B_{*j}=(v_{fj}^2-c_{*j}^2)/\rho_{*j}^4,\\
&B_{0j}=c_{*j}^2\rho_{*j}+B_{*j}\rho_{*j}^5/5-K_j\cdot[\rho_{*j}/(1-\alpha\rho_{*j}/\rho_m)],\\
&B_{1j}=K_j\cdot[\rho_{c2j}/(1-\alpha\rho_{c2j}/\rho_m)]+B_{0,j},\\
&c_{0j}=c_{\tau j},
\end{aligned}\right\} \tag{2.8}$$

further assuming $c/c_0=1$ when traffic density is above ρ_{c2j} to extend the VEM [1], the corresponding sound speed c_j can be written as

$$c_j=\begin{cases} \sqrt{c_{*j}^2+B_{*j}(\rho-\rho_{*j})^4} & \text{for } \rho\le\rho_{*j}, \\ K_j^{1/2}\cdot[1/(1-\alpha\rho/\rho_m)] & \text{for } \rho_{*j}<\rho\le\rho_{c2j}, \\ c_{\tau j}, & \text{otherwise.} \end{cases} \tag{2.9}$$

Therefore, using the definition of sound speed under isentropic condition in classical mechanics

$$c^2=\partial p/\partial\rho, \tag{2.10}$$

traffic pressure p_j can be written as

$$p_j=\begin{cases} c_{*j}^2\rho+\dfrac{1}{5}B_{*j}\cdot[\rho_{*j}^5+(\rho-\rho_{*j})^5] & \text{for } \rho\le\rho_{*j}, \\ K_j\cdot[\rho/(1-\alpha\rho/\rho_m)]+B_{0j} & \text{for } \rho_{*j}<\rho\le\rho_{c2j}, \\ c_{\tau j}^2(\rho-\rho_{c2j})+B_{1j}, & \text{otherwise,} \end{cases} \tag{2.11}$$

where traffic pressure p_j increases linearly with a slope $c_{\tau j}^2$ when $\rho>\rho_{c2j}$.

In this work, the density threshold of shock formation of vehicular flow due to the existence of the down-up hill road segment is particularly concerned, thus the free flow speed v_{f3} on uphill segment is allowed to be changeable. Assuming the second critical speed $u_{c2}=$ 18km/h, the $v_{f3}-$ dependencies of critical densities ρ_{*3}, ρ_{c23}, speed ratio $\Lambda_3(=c_{\tau 3}/u_{c2})$, and $q_e^{(1)}-\rho$ relationship can be obtained, as shown in Figs. 3(a)-(d). For a given value of ξ $[=(1-v_{f3}/v_{f2})]$, the braking distance $X_{\rm br3}$ in Fig. 3(c) or the 2nd column of Table 2 is determined simply by examining whether the $q_e^{(1)}-\rho$ curve is as smooth as the fundamental diagrams in Fig. 2. According to the values in the 2nd column of Table 2, in the considered range of ξ from 0.0833 to 0.3333, the braking distance $X_{\rm br3}$ in the unit of 100m can be expressed as

$$X_{\rm br3}=0.8133-0.9342\xi. \tag{2.12}$$

As shown in Figs. 4(a) and (b), the traffic density dependence of traffic sound speed ratio c/c_0 in part (a) and traffic pressure p in part (b) is calculated with respect to the road segment index krd. The blue-solid, black-solid and green-solid curves represent c/c_0 or p respectively for traffic flows on downhill, horizontal and uphill road segments. When the density is lower than the second critical density, the values of c/c_0 and p for uphill segment at a given traffic density are slightly higher, but the relevant values for downhill segment are slightly lower, with the values of p and c/c_0 for horizontal section located between the two.

It is noted that the model has used pressure gradient p_x/ρ in describing traffic acceleration R/ρ, suggesting that negative speeds in the solutions can possibly occur, as

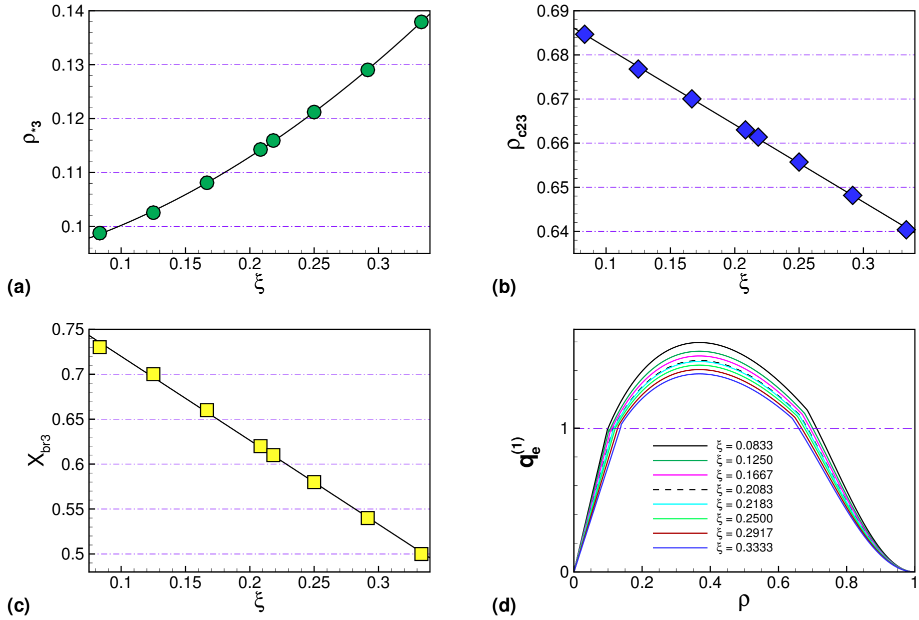

Figure 3: $\xi-$ dependencies of ρ_{*3} (a), ρ_{c23} (b), braking distance X_{br3} (c), and $q_e^{(1)}-\rho$ relationship (d). Note that $\xi=1-v_{f3}/v_{f2}$, ρ is measured by jam density ρ_m, X_{br3} has a unit of 100m, and $q_e^{(1)}$ is measured by $\rho_m v_{f2}^2$.

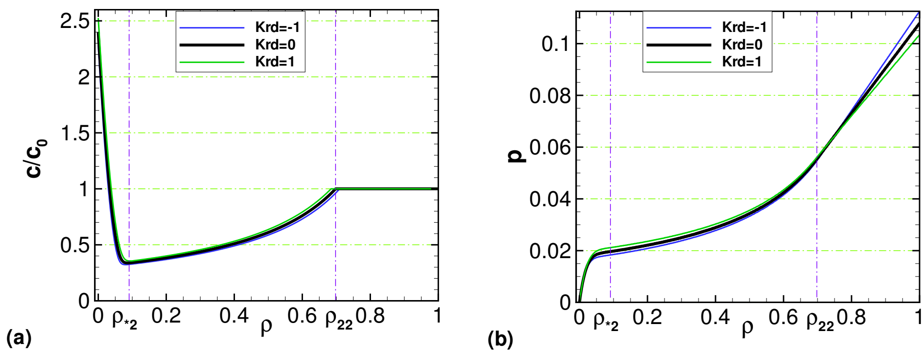

Figure 4: Density dependence of traffic sound speed ratio c/c_0 and traffic pressure p. Note that ρ is measured by jam density ρ_m, and p is measured by $\rho_m v_{f2}^2$.

reported by Aw and Rascle [17], which leads to the development of anisotropic higher-order traffic flow models (Rascle [18]; Xu et al. [19]).

In the VEM, what looks to be fresh is that three fundamental diagram curves are adopted in describing the ring road vehicular flow including down-up hill segment. Less is reported from a macroscopic point of view for the down-up hill effects on the spatial-temporal evolutions of ring vehicular flows and travel time through the ring. As

Table 2: $\xi-$ dependencies of some model parameters and the density threshold (ρ_0^+) of traffic shock formation.

ξ^*	X_{br3} (100m)	τ_{03} (s)	$c_{\tau 3}$ (v_0)	Λ_3	ρ_{*3} (ρ_m)	ρ_{c23} (ρ_m)	ρ_0^+ (ρ_m)
0.0833	0.73	7.8477	4.3556	2.6398	0.09877	0.68466	0.257
0.1250	0.70	8.2214	4.2266	2.5615	0.10256	0.67679	0.231
0.1667	0.66	8.6324	4.1205	2.4973	0.10811	0.67003	0.220
0.2083	0.62	9.0868	4.0148	2.4332	0.11428	0.66300	0.213
0.2183	0.61	9.2022	3.9909	2.4187	0.11594	0.66137	0.211
0.2500	0.58	9.5916	3.9095	2.3694	0.12121	0.65571	0.202
0.2917	0.54	10.1558	3.8051	2.3061	0.12903	0.64815	0.196
0.3333	0.50	10.7905	3.70183	2.2435	0.13793	0.64036	0.187

$*\ \xi=(v_{f2}-v_{f3})/v_{f2}$, is the relative difference of free flow speed.

reported [10], assuming the sound speed at zero density just equals to the free flow speed, i.e., $c=v_f$ for $\rho=0$, is certainly a favourable strategy for modeling the specific traffic stoppage problem specifically discussed by Daganzo [20], as it makes all the elements in the first column of Jacobian matrix as seen in Eq. (3.2) become zero, leading to the traffic flow q naturally totally not sensitive to the non-uniformity of density.

To predict the down-up hill segment effects on travel time through the ring road, as shown schematically in Fig. 1, the VEM is adopted in numerical simulation, with the model EZM also adopted to provide the counterpart results for comparison. In the simulation making use of EZM, the expressions for traffic sound speed and pressure are the same as that adopted in the VEM.

3 Numerical method

To solve the governing equations of the VEM, a fifth-order weighted essentially non-oscillatory scheme (WENO5) [11, 12] is adopted to calculate the numerical flux, and a 3rd order Runge-Kutta scheme (RK3) [13, 14] is used to handle time derivative terms. As the WENO5 is the same as reported by Zhang et al. [23], we will not repeat it here, and describe the numerical method in brief.

It is noted that the main reason for choosing the WENO5 scheme rather than other Riemann solvers is that essentially non-oscillatory (ENO) reconstruction [24] is based on adaptive stencils, such that the optimal stencil is chosen. This provides high-order accuracy and essentially non-oscillatory behavior. WENO reconstruction [13] consists of a convex combination of all the candidate stencils, and constitutes an improvement on ENO schemes on many levels, as reported by Johnsen and Colonius [25].

Defining $\partial p/\partial\rho=c^2$ and $p_x=c^2\rho_x$, and taking $R_1=R+p_x$ instead of R, the governing equations (2.1) and (2.2) can be written elegantly in the form

$$\frac{\partial \mathbf{U}}{\partial t}+\frac{\partial \mathbf{F}(\mathbf{U})}{\partial x}=\mathbf{S}, \tag{3.1}$$

where $\mathbf{U}=(\rho,q)^T$, $\mathbf{F}(\mathbf{U})=(q,q^2/\rho+p)^T$, and $\mathbf{S}=(0,R_1)^T$, with superscript 'T' representing vector transpose.

The eigenvalues of Eq. (3.1) λ_k, $(k=1,2)$ may be expressed as $\lambda_1=u-c$, and $\lambda_2=u+c$, where the Jacobian matrix is

$$\mathbf{A}=\begin{pmatrix} 0 & 1 \\ -u^2+c^2 & 2u \end{pmatrix}. \tag{3.2}$$

Further defining

$$\mathscr{L}(\mathbf{U})=-\frac{\partial\mathbf{F}(\mathbf{U})}{\partial\mathbf{x}}+\mathbf{S}, \tag{3.3}$$

to seek the numerical solution of

$$\frac{\partial\mathbf{U}}{\partial t}=\mathscr{L}(\mathbf{U}), \tag{3.4}$$

with the numerical flux $\widehat{\mathbf{F}}_{i+1/2}$ predicted by the WENO5 scheme [23], the RK3 scheme [13, 14] has the form

$$\begin{cases} \mathbf{U}_i^{(1)}=\mathbf{U}_i^n+\Delta t\mathscr{L}(\mathbf{U}_i^n), \\ \mathbf{U}_i^{(2)}=\dfrac{(3\mathbf{U}_i^n+\mathbf{U}_i^{(1)})}{4}+\dfrac{\Delta t\mathscr{L}(\mathbf{U}_i^{(1)})}{4}, \\ \mathbf{U}_i^{n+1}=\dfrac{(\mathbf{U}_i^n+2\mathbf{U}_i^{(2)})}{3}+\dfrac{2\Delta t\mathscr{L}(\mathbf{U}_i^{(2)})}{3}, \end{cases} \tag{3.5}$$

where the superscript n denotes time level.

Labeling the step ratio by $\omega=\Delta t/\Delta x$, the Courant–Friedrichs–Lewy (CFL) condition of the numerical method (WENO5+RK3) is given by

$$C_{\mathrm{FL}}=\omega\cdot\max|\lambda_{k,i}|<1, \quad k=1,2, \quad i=0,1,2,\cdots,I_{\max}-1, \tag{3.6}$$

where $\lambda_{k,i}$ represents the kth eigenvalue for $\mathbf{A}$ at x_i, $I_{\max}$ is the maximum number of node, the Courant number C_{FL} is assumed to be 0.7 [26] in the numerical tests to ensure numerical stability and calculate time step length Δt. Note that the numerical tests cannot obtain convergent results when the CFL condition is not fulfilled, as the RK3 scheme is explicit.

To increase the temporal discretization accuracy, source term linearization has been used previously [10, 27]. However, in the present numerical tests, without using source term linearization, we use the RK3 scheme with the total variation diminishing property [13, 14].

4 Density threshold definition and travel time prediction

4.1 Density threshold definition

In simulation, the initial density condition for ring road traffic flow is assumed to be

$$\rho(0,x)=\begin{cases} 1 & \text{for } x=\in[x_J-1/2,x_J+1/2], \\ \rho_0, & \text{otherwise}, \end{cases} \tag{4.1}$$

with $q(0,x)=q_e(\rho(0,x))$, where ρ_0 is the ring road initial density, x_J, $J=\mathrm{D,E,F}$ are the three positions of initial jams that are artificially assumed, their values are given in the caption of Fig. 1. Considering sags cause bottleneck effect, the onset of traffic shock at the density threshold (ρ_0^+) should result in density rise and traffic speed drop on the downhill segment, making downhill mean travel time $\sigma_{\text{tav}}^{(-1)}$ increases sharply. Hence, one method is to define ρ_0^+ by inspecting the variation tendency of $\sigma_{\text{tav}}^{(-1)}$ with ρ_0. Another method is to define ρ_0^+ by judging if there exist the onset of traffic shock through observing the spatiotemporal density evolution intuitively. We found that both methods can obtain the same value of density threshold ρ_0^+.

4.2 Travel time prediction

Numerical tests based on the VEM or EZM can provide the grid traffic speed $u(x_i,t^n)$. Following the previous work (Zhang, et al. [27]), using a pre-assigned time period Δ_0, the local average speed $\overline{u}_i(t)$ at the grid x_i can be calculated to predict travel time. The expression form is the same as reported [1], it should be omitted here.

5 Results and discussion

5.1 Simulation parameters and conditions

The numerical simulation uses uniform spatial grid, with a grid length fixed at $l_0=$ 100(m). Simulation parameters of ring road traffic flow are shown in Table 1. In the first column, for $j=1,2,3$, v_{fj} and $X_{\text{br}j}$ are the free flow speed and braking distance on the road segment j (see in Fig. 1), the value of τ_{0j} is obtained by assuming $\tau_{0j}=l_0/c_{\tau j}$, while $c_{\tau j}$ is calculated by Eq. (2.7) in the unit of v_0. In the second column, for $j=1,2,3$, the value of Λ_j is calculated by its definition $\Lambda_j=c_{\tau j}/u_{c2}$, ρ_{*j} and ρ_{c2j} are the first and second critical density on the road segment j, X_I for $I=\mathrm{A,B,C}$ are the positions of uphill ends.

In the third column of Table 1, l_0 is the grid length, X_I^{u} is the position of downhill starting point, L is the total length of the ring road, L_{h} is the length of downhill or uphill segment. ρ_m, l and u_{c2} are the jam density, the average length of vehicles and the second critical speed respectively, with v_0 and t_0 $(=l_0/v_0)$ being the speed and time scales in the simulation. When the free flow speed v_{f3} is changeable, the relevant values of some model parameters can be seen in the columns from the second to seventh of Table 2.

It was assumed that the Reynolds number ($\mathrm{Re}=l_0v_0/\nu$) is 64. The elasticity parameter $\widehat{\gamma}_2\{=\gamma_2/l_0^2=[0.68\times(l_0v_0/\mathrm{Re})\tau_{02}]/l_0^2\}$ equals 2.316×10^{-3} (Smirnova et al. [28, 29]). For ring road traffic flow, periodic boundary conditions can be applied.

5.2 Model validation

The model VEM is validated by the model EZM, which is not repeated here, as it has been reported previously [10]. In the flow simulation by the EZM, the expressions of traffic pressure and sound speed are the same as adopted in the VEM, and so are the numerical schemes for solving the EZM equations.

Travel time is a crucial indicator of the evolutions of ring road traffic flow. Table 3 shows the mean travel time σ_{tav}, the uphill and and downhill mean travel time $\sigma_{\mathrm{tav}}^{(\mathrm{krd})}$(krd$=1,-1$) at several values of ρ_0 for $L_{\mathrm{h}}=1$km. Comparing the values of sg_{tav} in the 2nd and 5th columns of Table 3, it is seen that the VEM can certainly predict much the same mean travel times. As shown in the 3rd and 4th columns of Table 3, the uphill mean travel time $\sigma_{\mathrm{tav}}^{(1)}$ and the downhill mean travel time $\sigma_{\mathrm{tav}}^{(-1)}$ estimated by the VEM are almost identical to those estimated by the EZM that can be seen in the 6th and 7th columns of Table 3. In particular, the downhill mean travel time $\sigma_{\mathrm{tav}}^{(-1)}$ is larger than the uphill mean travel time $\sigma_{\mathrm{tav}}^{(1)}$, even though on the downhill segment the traffic flow has a larger free flow speed v_{f1}.

The results consistency between the VEM and the EZM can be observed in the spatiotemporal evolution of traffic flow, as shown in Fig. 5. For $\rho_0=0.257$, the downhill road segment plays a role of vehicular aggregation, leading to onset of traffic shock, which causes traffic congestion. Overall, the right traffic flow pattern is almost the same as the left, suggesting that the numerical results based on the VEM are reliable.

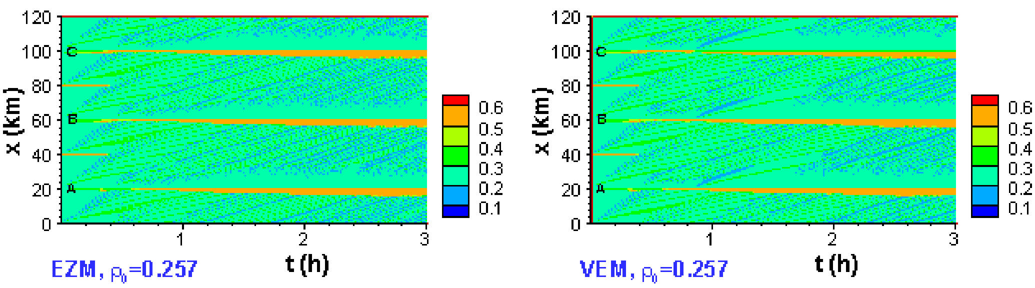

Figure 5: Spatial-temporal evolutions of traffic density on the ring road in the case of $\xi=0.0833$ and $\rho_0=0.257$.

Table 3: Density dependencies of $\sigma_{\rm tav}$ and $\sigma^{(\rm krd)}_{\rm tav}(\rm krd=1,-1)$ for $L_{\rm h}=1$km.

	VEM			EZM		
ρ_0	$\sigma_{\rm tav}$	$\sigma^{(1)}_{\rm tav}$	$\sigma^{(-1)}_{\rm tav}$	$\sigma_{\rm tav}$	$\sigma^{(1)}_{\rm tav}$	$\sigma^{(-1)}_{\rm tav}$
0.1	1.0824	0.0270	0.0314	1.0810	0.0269	0.0313
0.125	1.1766	0.0292	0.0341	1.1765	0.0292	0.0341
0.15	1.2840	0.0320	0.0379	1.2838	0.0321	0.0378
0.18	1.4229	0.0354	0.0424	1.4237	0.0353	0.0422
0.2	1.5192	0.0378	0.0461	1.5184	0.0377	0.0459
0.25	1.7656	0.0440	0.0575	1.7644	0.0441	0.0574
0.255	1.7907	0.0453	0.0619	1.7911	0.0451	0.0610
0.256	1.7962	0.0454	0.0630	1.7967	0.0453	0.0627
0.257	1.8366	0.0436	0.0952	1.8418	0.0437	0.0986
0.3	2.1174	0.0426	0.0755	2.0870	0.0442	0.0680
0.368	2.5517	0.0439	0.0629	2.5544	0.0437	0.0627
0.4	2.8436	0.0443	0.1016	2.7810	0.0453	0.0679
0.5	3.6143	0.0449	0.1041	3.6216	0.0448	0.1089
0.625	5.1149	0.1277	0.1374	5.1149	0.1277	0.1374

5.3 Transition of traffic flow pattern

Intuitively, near the density threshold of shock formation due to the existence of the down-up hill segment, ring road vehicular flow pattern illustrated by spatiotemporal evolution of traffic density should have a transition from a relatively smooth to a congested regime. Such an intuitive point of view is confirmed by the flow patterns demonstrated in Figs. 6(a)-(c), it is seen that with the decrease of relative difference of free flow speed ξ $[=(1-v_{f3}/v_{f2})]$, the pattern transition becomes more and more apparent, furthermore the density threshold ρ_0^+ becomes larger. For instance, if $\xi=0.3333$, $\rho_0^+=0.187$, while when ξ is 0.0833, the density threshold ρ_0^+ is 0.257.

To show clearly the impact of down-up hill segment on the ring road vehicular flow, distributions of traffic density and traffic speed at two instants $t=1$,2h in the case of $\xi=0.0833$ and $\rho_0=0.257$ are given by Figs. 7-8, where the starting points of downhill and uphill are labeled by dash-dot blue and red vertical line respectively, with the uphill ends labeled by dash green vertical line. From Figs. 7(a)-(b), it is seen that the traffic shock originates at the downhill end, and propagates backward. The occurrence of traffic shock results in the drop the traffic speed, accordingly there is the so-called sags' bottleneck effect causing capacity reduction.

5.4 Comparison with measured data

The instantaneous traffic speed (u) and equilibrium speed (u_e) at $X=60$km for $\rho_0=0.18$, 0.3 are plotted as a function of local traffic density in Figs. 9(a)-(b), but part (c) of Fig. 9 is used to compare the speed-flow u-q relationship at a downhill mid point $X=59.5$

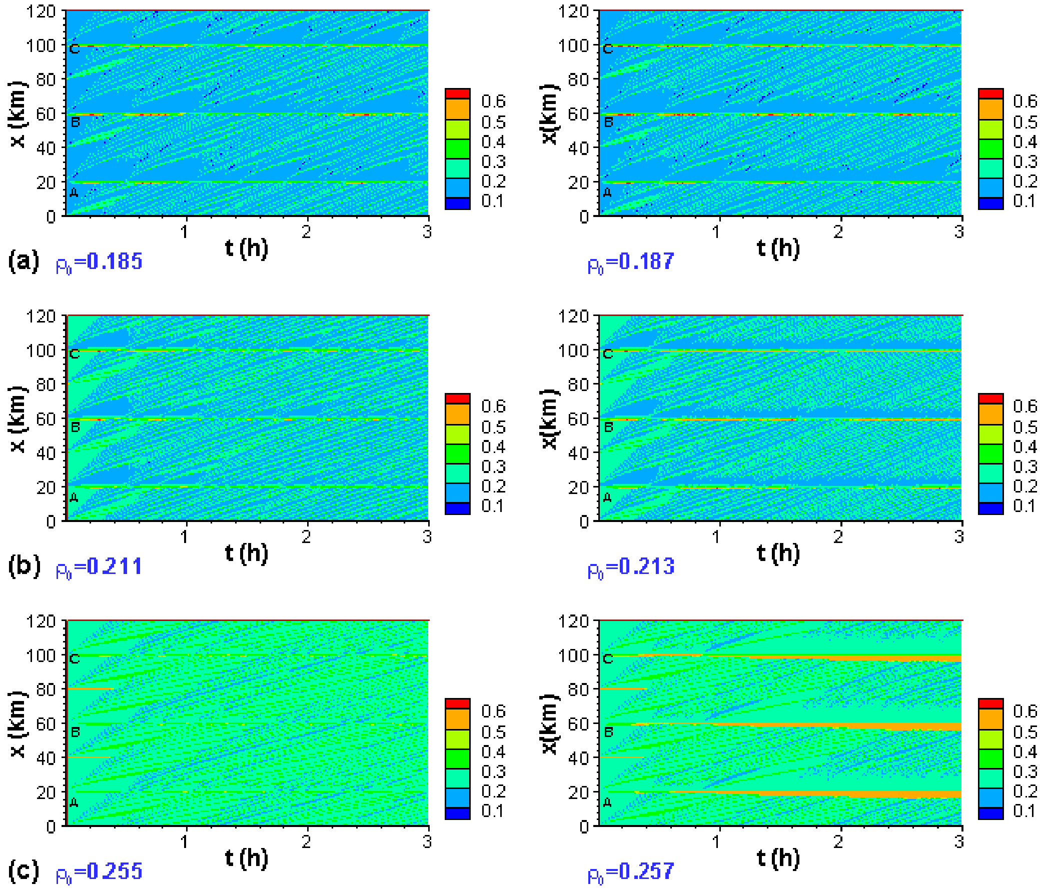

Figure 6: Spatial-temporal evolutions of traffic density on the ring road for (a) $\xi = 0.3333$; (b) $\xi = 0.2083$; (c) $\xi = 0.08333$.

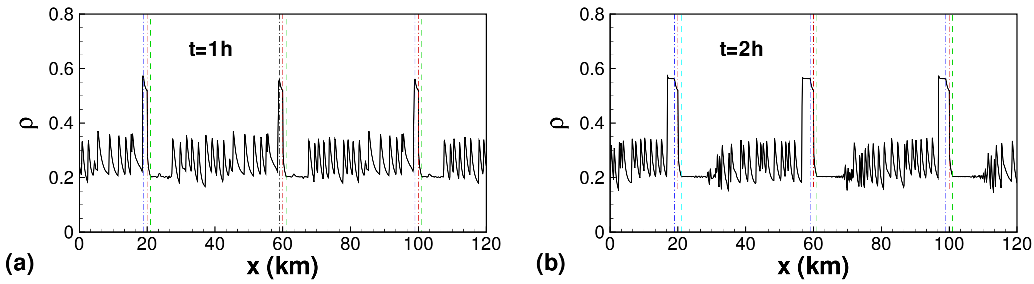

Figure 7: Distribution of traffic density ρ on the ring road for $\xi = 0.0833$, $\rho_0 = 0.257$ at (a) $t = 1$h, (b) $t = 2$h.

with field observation data. As the segment index $krd = -1$ at $X = 60$km, the instantaneous equilibrium speed u_e is calculated with the blue-colored fundamental diagram

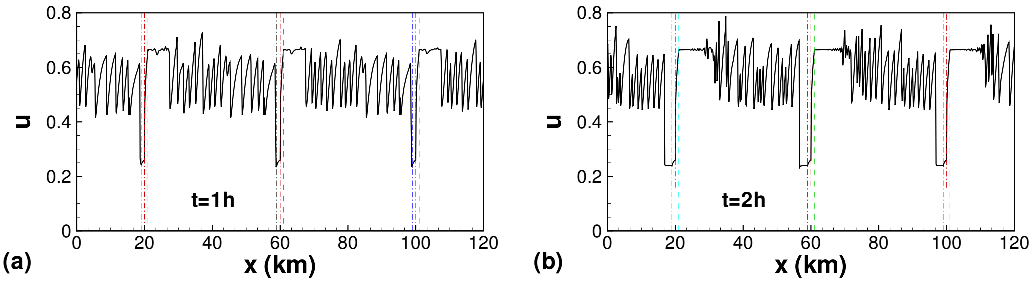

Figure 8: Distribution of traffic speed u on the ring road for $\xi=0.0833$, $\rho_0=0.257$ at (a) $t=1$h, (b) $t=2$h.

curve given by Fig. 2, the speed u_e is labeled by unfilled blue-triangles, some observation date extracted from McShane, Roess and Prassas [30] are labeled by symbol $'+'$ in parts (a)-(c), with other measured data extracted from Patire and Cassidy [31] also labeled by symbol $'+'$ in part (d).

For $\rho_0=0.18$, traffic speed u are calculated by the VEM using the 3rd order Runge-Kutta method with the WENO5 scheme adopted for predicting the numerical flux. As shown in Fig. 8(a), the $u-\rho$ relationship depends on ξ value; almost all the traffic flow points (ρ,u) fall within the range of measured data points, the calculated speed under the unsaturated initial condition has taken some value almost completely in the range of measured data, suggesting that numerical results based on the VEM are basically reliable.

From Fig. 9(b), for $\rho_0=0.3$, it is seen that decreasing ξ can enhance the variation range of density and speed. All flow points (ρ,u) are located in the scattered region of measured data.

In Fig. 9(d), the measured data for median lane were recorded on December 23 of 2005, time-of-day tags from 6:30 to 7:10 hours, at the site of the Tomei expressway (near Tokyo) instrumented with a series of eleven video cameras and two sets of loop detectors at kilo-post (KP) 21.5 [31]. It is seen that for $\rho_0=0.15$, 0.25, and 0.3, almost all of the traffic flow points predicted by the VEM at the downhill mid point fall in the scattered region of observed data points. The comparison shows a good consistency with the measured data.

5.5 Travel time

Different from that reported by Chang and Mahmassani [32], who have examined two heuristic rules proposed for describing urban commuters' predictions of travel time as well as the adjustments of departure time in response to unacceptable arrivals in their daily commute under limited information, here we discuss the impacts of down-up hill segment on the travel time through the ring road on the basis of the EZM and VEM, as travel time is a crucial indicator of traffic flow performances.

The ρ_0- dependencies of mean travel time $\sigma_{\rm tav}$ (in a unit of L/v_{f2}), its rms value $\sigma_{\rm t}'$,

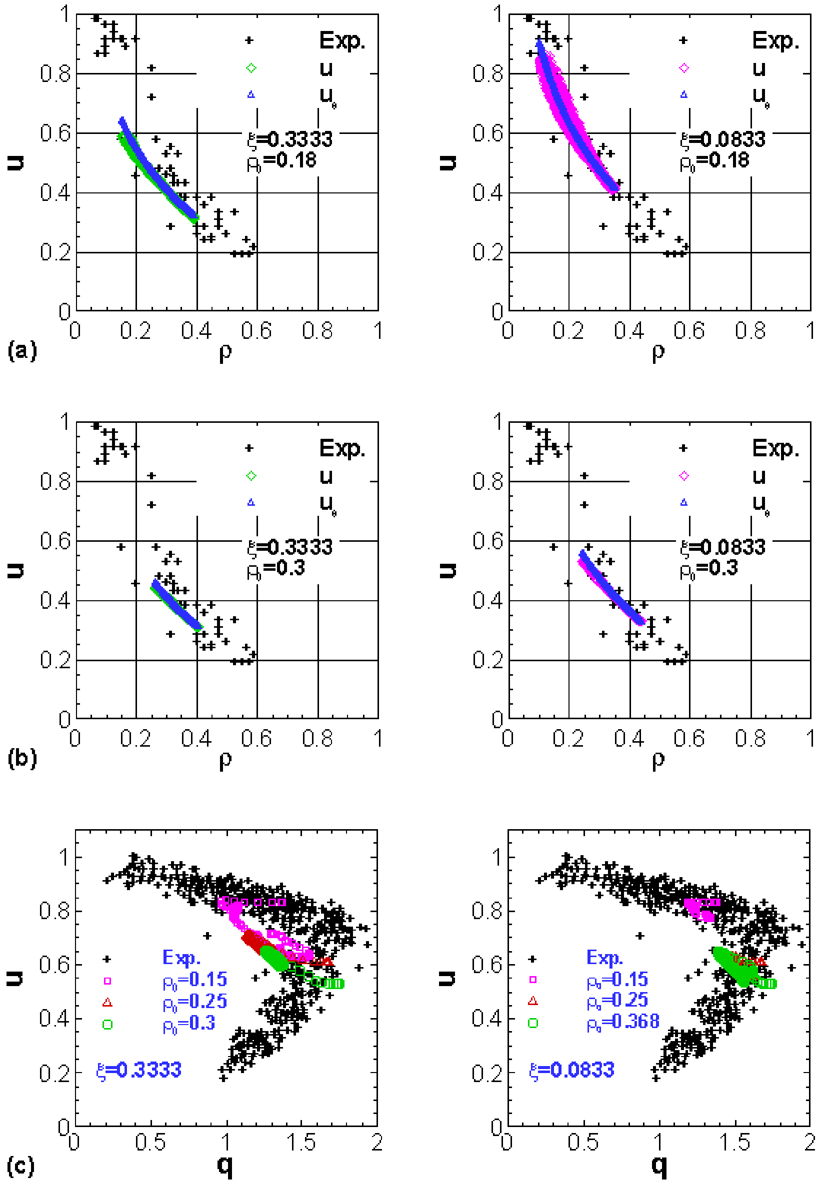

Figure 9: Comparison of traffic speed with existing measured data for $\xi=0.3333, 0.0833$ in the case of $L_h=1$km, (a) ρ_0=0.257; (b) ρ_0=0.368 at $x=60$km; and (c) Comparison of the instantaneous u-q relationship at the downhill midpoint $x=59.5$km with field observation data. The observation data used in parts (a) and (b) are obtained from McShane, Roess and Prassas [30], and the jam density for normalization is assumed to be 200veh/mile; For the convenience of showing the field data from Patire and Cassidy [31], the speed and flow rate for normalization are respectively assumed to be $130\text{km/h}[v_{fe}=(v_{f1}+v_{f2})/2]$, and 1465vph $[\approx v_{fe}\times(\rho_m\rho_{*2})]$.

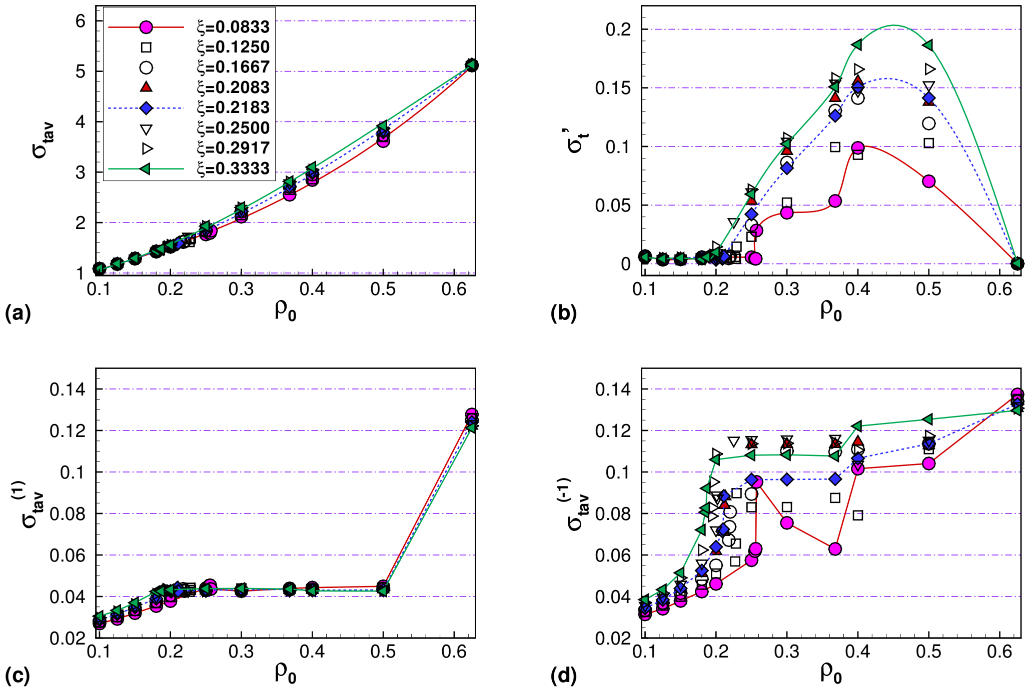

Figure 10: Density dependencies of mean travel time $\sigma_{\rm tav}$ (a), its rms value $\sigma_{\rm t}^{'}$ (b), uphill mean travel time $\sigma_{\rm tav}^{(1)}$ (c), and downhill mean travel time $\sigma_{\rm tav}^{(1)}$ (d) at different value of ξ.

uphill mean travel time $\sigma_{\rm tav}^{(1)}$ and downhill mean travel time $\sigma_{\rm tav}^{(-1)}$ are shown in Figs. 9(a)-(d). Examining Fig. 10(a), it is seen that the mean travel time $\sigma_{\rm tav}$ increases with the initial density monotonically. With the increase of ξ $[=(1-v_{f3}/v_{f2})]$, when the density is in the range from the density threshold ρ_0^+ to 0.5, ring road traffic flow has traffic shock generated by the down-uphill segment, the mean travel time increases observably. Using a 3rd order polynomial fitting in the following form

$$\sigma_{\rm tf}=c_0+c_1\rho_0+c_2\rho_0^2+c_3\rho_0^3, \tag{5.1}$$

one yields

$$\begin{pmatrix} c_0 & c_1 \\ c_2 & c_3 \end{pmatrix}_{\xi=0.0833}=\begin{pmatrix} 0.68775 & 3.60830 \\ 1.57089 & 6.32250 \end{pmatrix}, \tag{5.2a}$$

$$\begin{pmatrix} c_0 & c_1 \\ c_2 & c_3 \end{pmatrix}_{\xi=0.3333}=\begin{pmatrix} 0.77608 & 1.5685 \\ 13.7579 & -8.2363 \end{pmatrix}. \tag{5.2b}$$

As can be seen in Fig. 10(b), $\sigma_{\rm t}'$ is rather sensitive to the density threshold of shock formation ρ_0^+, when ρ_0 is below ρ_0^+, σ_t' is rather small but has an obvious jump in the case of $\rho_0=\rho_0^+$, such as shown by the red curve with purple-color filled circles relevant to to the line legend $\xi=0.0833$. For the case of $\rho_0=0.625$, $\sigma_{\rm t}'$ closes to zero. If ρ_0 is in the range from ρ_0^+ to 0.5, the variation of $\sigma_{\rm t}'$ with the density ρ_0 is determined by the value of ξ, in general σ_t' is below 0.2.

As shown in Fig. 10(c), when ρ_0 is below ρ_0^+, the uphill mean travel time $\sigma_{\rm tav}^{(1)}$ increases almost linearly. When $\rho_0=\rho_0^+$, $\sigma_{\rm tav}^{(1)}$ reaches a value that does not vary with ρ_0 until $\rho_0>0.5$. This is because the down-up hill segment has generated a traffic shock originating at the downhill end. However, the variation of $\sigma_{\rm tav}^{(-1)}$ with the density ρ_0 is obviously sensitive to the value of ξ, as shown in Fig. 10(d). In particular, there is a apparent jump of downhill mean travel time $\sigma_{\rm tav}^{(-1)}$ in the case of $\rho_0=\rho_0^+$. For instance, when $\xi=0.2183$, the jump height is 0.16 when the density ρ_0 changes from 0.210 to $\rho_0^+|_{\xi=0.2183}=0.211$, as illustrated by the dashed curve labeled by blue color filled diamonds in in Fig. 10(d). In general, in addition to the much dense case $\rho_0=0.625$, it is seen that when ρ_0 is above the threshold ρ_0^+, the downhill mean travel time $\sigma_{\rm tav}^{(-1)}$ is much larger than the uphill mean travel time $\sigma_{\rm tav}^{(1)}$.

5.6 Density threshold

The density threshold reflects a road condition under which down-up hill segment has just originated a traffic shock, causing the occurrence of sags' bottleneck effect. In this work, the threshold is determined by numerical simulation of ring road traffic flows on a platform built on the bases of the VEM. It is determined by examining the variation of downhill mean travel time with density ρ_0 or the spatiotemporal evolution of traffic density to seek if traffic shock has been generated by the down-up hill segment.

Corresponding to the sound speed $c_{\tau 3}$ given by Fig. 11(a), from Fig. 11(b), one can see that the numerically predicted density threshold of shock formation decreases monotonically with the increase of the relative difference of free flow speed ξ $(=1-v_{f3}/v_{f2})$.

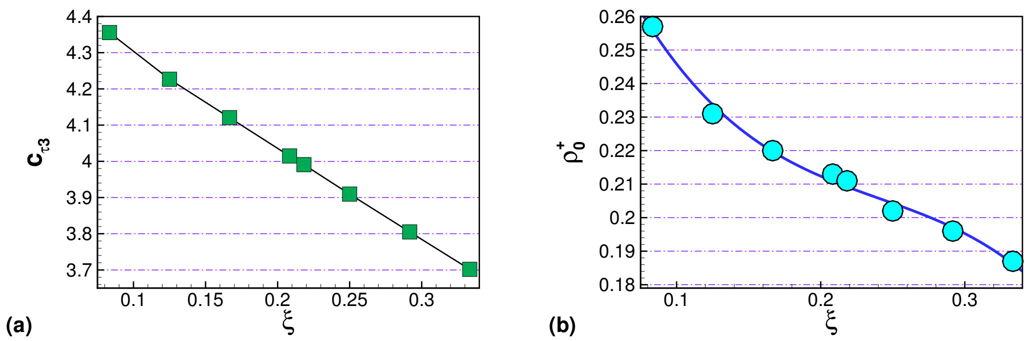

Figure 11: $\xi-$ dependencies of $c_{\tau 3}$ (a) and the density threshold ρ_0^+ (b) of traffic shock formation.

Using a 3rd order polynomial fitting, one obtains

$$\rho_0^+ = 0.3360 - 1.3194\xi + 4.8495\xi^2 - 6.7174\xi^3, \quad \xi \in [0.0833, 0.3333], \tag{5.3}$$

which can predict a density threshold ρ_0^+ of shock formation of ring road vehicular flow under the given range of ξ.

6 Conclusions

To explore the impacts of down-up hill segment on the density threshold of shock formation in ring road vehicular flow, a viscoelastic continuum model VEM is extended and used. Based on the VEM, a WENO5 scheme and a 3rd order Runge-Kutta scheme are adopted to build a simulation platform. The numerical simulation has the following conclusions:

1. Traffic pressure can be derived by assuming the traffic sound speed at first and then using the sound definition in classical mechanics. With the explicit algebraic traffic pressure and sound speed, the VEM can predict the mean travel time, the downhill mean travel time and uphill mean travel time much the same as the Navier-Stokes like model extended as EZM. In addition to the model comparison, the numerically estimated traffic state points are found to fall in the scattered region of field observation data. This validation indicates the numerical results based on the VEM is reliable.

2. The density threshold of shock formation by the down-up hill segment can be simply determined either by observing the spatiotemporal evolution of traffic density to seek if there is traffic congestion near the down-up hill or by examining the variation of the downhill mean travel time with initial density. The threshold of shock formation relies on the assumptions of modelling, but the existence of threshold to some extent can deepen the understanding of the impacts of down-up hill segment on vehicular flow and improve traffic management strategies.

3. With the increase of the relative difference of free flow speed, the mean travel time becomes larger particularly when the initial density is beyond the density threshold of traffic shock formation; the threshold decreases approximately in a third order polynomial way when the relative difference is in the range from 0.0833 to 0.3333.

4. The traffic shock is originated at the downhill end and propagates backward. In comparison with the downhill mean travel time and the uphill mean travel time, the former is generally larger and much more sensitive to the relative difference of free flow speed.

Acknowledgements

This work is supported by National Natural Science Foundation of China (NSFC No. 11972341) and fundamental research project of Lomonosov Moscow State University's Mathematical models for multi-phase media and wave processes in natural, technical and social systems. We thank Professor Gong Li at USTC and Dr. Yinglin Li at Peking University for some useful private communications.

References

[1] Z. J. Hu, M. N. Smirnova, Y. L. Zhang, N. N. Smirnov, and Z. J. Zhu, *Estimation of travel time through a composite ring road by a viscoelastic traffic flow model,* Math. Comput. Simul., 181 (2021), pp. 501–521.

[2] H. M. Zhang, *Driver memory, traffic viscosity and a viscous vehicular traffic flow model,* Transp. Res. Part B Methodol., 37 (2003), pp. 27–41.

[3] A. D. Patire, and M. J. Cassidy, *Lane changing patterns of bane and benefit: Observations of an uphill expressway,* Transp. Res. Part B Methodol., 45 (2011), pp. 656–666.

[4] B. Goñi-Ros, V. L. Knoop, B. van Arem, and S. P. Hoogendoorn, *Empirical analysis of the causes of stop-and-go waves at sags,* IET Intelligent Transport Systems, 8(5) (2014a), pp. 499–506.

[5] B. Goñi-Ros, V. L. Knoop, B. van Arem, and S. P. Hoogendoorn, *Mainstream traffic flow control at sags,* Transp. Res. Rec. J. Transp. Rec. Board, 2470(1) (2014b), pp. 57–64.

[6] B. Goñi-Ros, V. L. Knoop, Y. Shiomi, T. Takahashi, B. van Arem, and S. P. Hoogendoorn, *Lane changing patterns of bane and benefit: Observations of an uphill expressway,* Int. J. Intel. Transp. Syst. Res., 14(1) (2016a), pp. 64–74.

[7] B. Goñi-Ros, V. L. Knoop, T. Takahashi, I. Sakata, B. van Arem, and S. P. Hoogendoorn, *Optimization of traffic flow at freeway sags by controlling the acceleration of vehicles equipped with in-car systems,* Transp. Res. Part C Emerg. Tech., 71 (2016b), pp. 1–18.

[8] W. L. Jin, and H. M. Zhang, *The formation and structure of vehicle clusters in the payne-whitham traffic flow model,* Transp. Res. Part B Methodol., 37(3) (2003), pp. 207–223.

[9] A. B. Kiselev, V. F. Nikitin, N. N. Smirnov, and M. V. Yumashev, *Irregular traffic flow on a ring road,* J. Appl. Math. Mech., 64(4) (2000), pp. 627-634.

[10] Y. L. Zhang, M. N. Smirnova, A. I. Bogdanova, Z. J. Zhu, and N. N. Smirnov, *Travel time prediction with a viscoelastic traffic model,* Appl. Math. Mech., 39(12) (2018a), pp. 1769–1788.

[11] G. S. Jiang, and C. W. Shu, *Efficient implementation of weighted eno schemes,* J. Comput. Phys., 126 (1996), pp. 202–228.

[12] A. K. Henrick, T. D. Aslam, and J. M. Powers, *Mapped weighted essentially non-oscillatory schemes: Achieving optimal order near critical points,* J. Comput. Phys., 207 (2005), pp. 542–567.

[13] C. W. Shu, *Total-variation-diminishing time discretizations,* SIAM J. Sci. Stat. Comput., 9 (1988), pp. 1073–1084.

[14] C. W. Shu, and S. Osher, *Efficient implementation of essentially non-oscillatory shock-capturing schemes,* J. Comput. Phys., 83 (1989), pp. 32–78.

[15] D. Helbing, and M. Treiber, *Gas-kinetic-based traffic model explaining observed hysteretic phase transition,* Phys. Rev. Lett., 81 (1998), pp. 3042–3045.

[16] S. P. Hoogendoorn, and P. H. L. Bovy, *Continuum modeling of multiclass traffic flow,* Transp. Res. Part B Methodol., 34(2) (2000), pp. 123–146.
[17] A. Aw, and M. Rascle, *Resurrection of second order models of traffic flow,* SIAM J. Appl. Math., 60 (2000), pp. 916–938.
[18] M. Rascle, *An improved macroscopic model of traffic flow: derivation and links with the Lighthill-Whitham model,* Math. Comput. Model., 35 (2000), pp. 581–590.
[19] R. Y. Xu, P. Zhang, S. C. Dai, and S. C. Wong, *Admissibility of a wide cluster solution in anisotropic higher-order traffic flow models,* SIAM J. Appl. Math., 68(2) (2007), pp. 562–573.
[20] C. F. Daganzo, *Requiem for second-order fluid approximations of traffic flow,* Transp. Res. Part B Methodol., 29 (1995), pp. 277–286.
[21] Z. J. Zhu, and C. Yang, *Visco-elastic traffic flow model,* J. Adv. Transp., 47 (2013), pp. 635–649.
[22] J. Ma, C. K. Chan, Z. B. Ye, and Z. J. Zhu, *Effects of maximum relaxation in viscoelastic traffic flow modeling,* Transp. Res. Part B Methodol., 113 (2018), pp. 143–163.
[23] Y. L. Zhang, M. N. Smirno *va, J. Ma, Z. J. Zhu, and N. N. Smirnov, Freeway tunnel effect of travel time based-on a double lane traffic model,* Int. J. Transp. Sci. Tech., (2021).
[24] C. W. Shu, and S. Osher, *Efficient implementation of essentially non-oscillatory shock-capturing schemes,* J. Comput. Phys., 77 (1988), pp. 439–471.
[25] E. Johnsen, and T. Colonius, *Implementation of WENO schemes in compressible multicomponent flow problems,* J. Comput. Phys., 219 (2006), pp. 715–732.
[26] H. S. Shui, TVD scheme, H. S. Shui (ed.) Finite Difference in One-dimensional Fluid Mechanics, National Defense: Beijing, in Chinese, 1998, pp. 333–355.
[27] Y. L. Zhang, M. N. Smirnova, A. I. Bogdanova, Z. J. Zhu, and N. N. Smirnov, *Travel time estimation by urgent-gentle class traffic flow model,* Transp. Res. Part B Methodol., 113 (2018), pp. 121–142.
[28] M. N. Smirnova, A. I. Bogdanova, Z. J. Zhu, and N. N. Smirnov, *Traffic flow sensitivity to visco-elasticity,* Theor. Appl. Mech. Lett., 6 (2016), pp. 182–185.
[29] M. N. Smirnova, A. I. Bogdanova, Z. J. Zhu, and N. N. Smirnov, *Traffic flow sensitivity to parameters in viscoelastic modelling,* Transp. B Transp. Dyn., 5(1) (2017), pp. 115–131.
[30] W. R. McShane, R. P. Roess, and E. S. Prassas, *Calibration Relationships for Freeway Analysis,* in W. R. McShane, R. P. Roess, and E. S. Prassas (eds.) Traffic Engineering, Prentice-Hall: New Jersey, 1998. pp. 282–306.
[31] A. D. Patire, and M. J. Cassidy, *Observations of lane changing patterns on an uphill expressway,* (2010), URL `https://escholarship.org/uc/item/4mr9m6sz`.
[32] G. L. Chang, and H. S. Mahmassani, *Travel time prediction and departure time adjustment behavior dynamics in a congested traffic system,* Transp. Res. Part B Methodol., 22(2) (1988), pp. 217–232.